



Cite this: *New J. Chem.*, 2019, 43, 13985

# Liquid phase hydrogenation of CO<sub>2</sub> to formate using palladium and ruthenium nanoparticles supported on molybdenum carbide†

Claire E. Mitchell,<sup>a</sup> Umberto Terranova,<sup>a</sup> Ihfaf Alshibane,<sup>b</sup> David J. Morgan,<sup>a</sup> Thomas E. Davies,<sup>a</sup> Qian He,<sup>a</sup> Justin S. J. Hargreaves,<sup>b</sup> Meenakshisundaram Sankar<sup>a\*</sup> and Nora H. de Leeuw<sup>a\*</sup>

We report the development of palladium nanoparticles supported on Mo<sub>2</sub>C as an active catalyst for the liquid-phase hydrogenation of CO<sub>2</sub> to formate under mild reaction conditions (100 °C and 2.0 MPa of a 1:1 CO<sub>2</sub>:H<sub>2</sub> mixture). A series of Pd/Mo<sub>2</sub>C catalysts were synthesised via the modified wet-impregnation (MIm) and sol-immobilization (SIm) techniques and evaluated for CO<sub>2</sub> hydrogenation, in an aqueous 1 M NaOH solution. MIm catalysts synthesised using PdCl<sub>2</sub> dissolved in a 2 M HCl solution gave the highest formate yield with turnover numbers of up to 109 after 19 h. We further report the crucial role of base and the pH of the reaction medium for the hydrogenation of CO<sub>2</sub> to formate. Based on stability studies, electron microscopic characterisation and density functional theory calculations we found that Ru has a stronger affinity than Pd to Mo<sub>2</sub>C resulting in the development of a stable bimetallic RuPd/Mo<sub>2</sub>C catalyst for the hydrogenation of CO<sub>2</sub> to formate.

Received 24th April 2019,  
Accepted 1st August 2019

DOI: 10.1039/c9nj02114k

rsc.li/njc

## Introduction

The growing demand for natural gas and petroleum based feedstock for power generation, transport and chemicals production has, in recent decades, resulted in an unsustainable increase in CO<sub>2</sub> emissions.<sup>1,2</sup> Irreversible climate change, diminishing conventional fossil fuel reserves and the complexities involved in extracting unconventional fossil reserves, are driving the development of sustainable, renewable and non-fossil-based feedstock for the production of chemicals and fuels. In spite of its thermodynamic stability, carbon dioxide has become an attractive C-1 feedstock for the production of chemicals and fuels.<sup>3–5</sup> With the recent advances in carbon capture technologies, cost-competitive pure CO<sub>2</sub> could become available for its conversion to value-added chemicals.<sup>6</sup> Economically sustainable large-scale CO<sub>2</sub> conversion could help in achieving the emission targets set out in the Paris Agreement<sup>7</sup> while increasing the production of chemicals and fuels.

Commercially, CO<sub>2</sub> utilisation is thus far limited to the production of a few chemicals, including urea<sup>8</sup> (for nitrogen fertilizers and plastics), polycarbonates<sup>9</sup> (for plastics), salicylic acid (a pharmaceutical ingredient)<sup>10</sup> and methanol.<sup>5</sup> Among all

the possible transformations, CO<sub>2</sub> hydrogenation to acids, alcohols and hydrocarbons using H<sub>2</sub> derived from non-fossil feedstock (e.g. water splitting using electricity derived from a renewable source) is the most promising strategy.<sup>11</sup> Here, it is important to note that recently tremendous progress has been made in the production of H<sub>2</sub> via water-splitting using electricity.<sup>12</sup> CO<sub>2</sub> hydrogenation is challenging because of the inherent thermodynamic stability of CO<sub>2</sub> along with the lack of active catalysts that can activate CO<sub>2</sub> under reasonable reaction conditions.<sup>4</sup> However, the potential of such an abundant feedstock for producing organic compounds, coupled with the possibility of balancing CO<sub>2</sub> emissions make CO<sub>2</sub> hydrogenation an exciting and challenging topic for research.

An important product that is formed from the hydrogenation of CO<sub>2</sub> is formic acid, which is a liquid at room temperature and contains 4.4 wt% of hydrogen.<sup>13</sup> Current annual production of formic acid is around 600 000 tons and this is projected to grow by 22% annually.<sup>14</sup> Formic acid is a vital intermediate in many industries including dyeing, leather, food, agrochemical and many more.<sup>15–17</sup> It is also used to promote the fermentation of acetic acid, as a coagulant in rubber synthesis, an antibacterial agent in animal feed and as a de-icing agent in many manufacturing industries.<sup>18</sup> Using appropriate catalysts, formic acid can be controllably converted to CO<sub>2</sub> and H<sub>2</sub> even at room temperature.<sup>19</sup> Hence, hydrogenation of CO<sub>2</sub> to formic acid is considered as an effective strategy to store H<sub>2</sub> chemically. Current technology for the production of formic acid involves

<sup>a</sup> Cardiff Catalysis Institute, School of Chemistry, Cardiff University, Cardiff CF10 4AT, UK. E-mail: Sankar@cardiff.ac.uk, deleeuw@cardiff.ac.uk

<sup>b</sup> School of Chemistry, Glasgow University, Glasgow G12 8QQ, UK

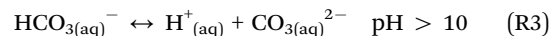
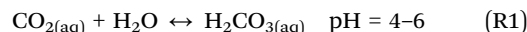
† Electronic supplementary information (ESI) available. See DOI: 10.1039/c9nj02114k

the hydrolysis of methyl formate, with a capacity of *ca.* 770 kilotons per annum in 2014.<sup>20</sup> Limitations of this process include the use of fossil fuel based feedstock, slow reaction rate, undesirable by-products and high cost. Therefore, it is not surprising that utilization of CO<sub>2</sub> is gaining momentum in the scientific community in order to shift from conventional fossil-based processes toward environment-friendly direct hydrogenation of CO<sub>2</sub> to formic acid.

Most of the reported catalysts for the hydrogenation of CO<sub>2</sub> to formic acid are homogeneous metal (Rh, Ru, Ir and Fe) complexes containing sophisticated ligands (N-heterocyclic carbenes, pincer ligands and phosphines) that require complicated synthesis and/or handling procedures.<sup>21–24</sup> Although these homogeneous catalysts are highly active, heterogeneous catalysts are preferred for a number of reasons, *e.g.* catalyst separation and scalability. Transition metal carbides have been reported to exhibit catalytic activities for a number of chemical reactions, including CO hydrogenation,<sup>25</sup> the water gas shift reaction,<sup>26</sup> hydrodesulphurization<sup>27</sup> and methane reforming.<sup>28</sup> Recently, transition metal carbides have also been reported as catalysts for CO<sub>2</sub> hydrogenation<sup>29</sup> including by Dubois *et al.*<sup>30</sup> and Vidal *et al.*<sup>31</sup> All these reactions were carried out at relatively high temperatures (220–320 °C), and mostly in the gas-phase, where the most interesting products like CH<sub>3</sub>OH or HCOOH are thermodynamically not favoured.<sup>32,33</sup> Hence, it is desirable to perform the hydrogenation of CO<sub>2</sub> at lower temperatures where CO (a product from an endothermic reaction) is not favoured.

Chen *et al.* demonstrated this by performing CO<sub>2</sub> hydrogenation at 200 °C in the liquid phase for the production of MeOH, they reported catalysis using metal nanoparticles supported on Mo<sub>2</sub>C using 1,4-dioxane as the solvent.<sup>34,35</sup> They synthesized a series of M/Mo<sub>2</sub>C (M = Pd, Cu, Co and Fe) catalysts, for the formation of CH<sub>3</sub>OH, C<sub>2</sub>H<sub>5</sub>OH and C<sub>2+</sub> hydrocarbons. 1,4-Dioxane however, is not an environmentally-benign solvent of choice,<sup>36</sup> other organic solvents have also been reported for the liquid phase hydrogenation of CO<sub>2</sub>, including ethanol.<sup>37</sup> Organic solvents have the disadvantage of being involved in the reaction itself, and may play a role in the synthesis of the targeted products; hence, it is better to avoid using them. It has been reported that addition of water is effective for improving CO<sub>2</sub> hydrogenation to formic acid.<sup>38,39</sup> It is proposed that the hydrogen-bonding between the H<sub>2</sub>O molecule and CO<sub>2</sub> improves the electrophilicity of the carbon atom on the CO<sub>2</sub> molecule,<sup>39</sup> thus reducing the reaction barrier for CO<sub>2</sub> activation. The same group reported Mo<sub>2</sub>C acted as a co-catalyst as well as a support as it performed CO<sub>2</sub> conversion without any other metals present. Posada-Perez *et al.* compliment this by explaining that the specific carbon/metal ratio of Mo<sub>2</sub>C is responsible for the high reactivity resulting in the breaking of both C–O bonds in CO<sub>2</sub> before hydrogenation.<sup>40</sup> Mori *et al.* reported the formation of formic acid from CO<sub>2</sub> hydrogenation using a ruthenium-based catalyst, in water under alkaline conditions at 100 °C,<sup>41</sup> Song *et al.* also reported hydrogenation of CO<sub>2</sub> to formic acid in water using a Na<sub>2</sub>CO<sub>3</sub> base, catalysed by palladium supported on chitin.<sup>42</sup> These alkaline conditions are important in improving the CO<sub>2</sub> solubility in water. CO<sub>2</sub> has poor solubility in pure water (0.0693 mol kg<sup>−1</sup> at 1 bar at 30 °C)<sup>43</sup> and the solubility decreases with increasing temperature. Carbonic

acid (H<sub>2</sub>CO<sub>3</sub>), formed when CO<sub>2</sub> dissolves in water, deprotonates sequentially to form the carbonate ion (eqn (R1)–(R3)).



Because of these equilibria, different species dominate the aqueous medium at different pH,<sup>44</sup> as noted above. Consequently, pH is an important parameter in this reaction, especially for the dissolution of CO<sub>2</sub> in the reaction medium. There are very few other reported catalysts for CO<sub>2</sub> hydrogenation to formic acid under aqueous alkaline conditions, these have been listed in the ESI† (Table S1). In the literature, NaHCO<sub>3</sub> and Na<sub>2</sub>CO<sub>3</sub> have been reported to increase the pH and hence improve the dissolution of CO<sub>2</sub> into the aqueous medium.<sup>41,45–47</sup> However, NaHCO<sub>3</sub> alone, without any added CO<sub>2</sub>, produces formic acid under hydrogenation conditions (*vide infra* Fig. 2). Hence, it is very important to choose the most appropriate base.

Plausible mechanisms for formation of formic acid from CO<sub>2</sub> hydrogenation has been widely investigated.<sup>48–52</sup> H<sub>2</sub> is a non-polar molecule, therefore is not very soluble in water as it does not readily form hydrogen bonds with water. It has been widely reported that Pd readily adsorbs and dissociates H<sub>2</sub> gaseous molecules.<sup>53–55</sup> In fact, Wang *et al.* found that H<sub>2</sub> chemisorption increased when Pd was supported on Mo<sub>2</sub>C in comparison with Pd supported on Al<sub>2</sub>O<sub>3</sub> due to additional chemisorption onto the Mo<sub>2</sub>C support<sup>56</sup> likely due to the strong electronic interaction between the β-Mo and H<sub>2</sub> (−0.67 eV).<sup>57</sup> Wang *et al.* studied palladium nanoparticles supported on nitrogen-doped mesoporous carbon in aqueous conditions.<sup>49</sup> Here they report the metallic palladium nanoclusters help the dissociative adsorption of H from H<sub>2</sub>. The resulting Pd–H bond activates the adsorbed bicarbonate by inserting the adsorbed H into the C–OH group of the bicarbonate, replacing the –OH which then binds with the remaining adsorbed H to form water. These findings are within good agreement with He *et al.*<sup>50</sup> and also Mori and co-workers work<sup>51</sup> all within aqueous conditions. Using systematic calculations, both of these papers go on to explain that the reduction of HCO<sub>3</sub><sup>−</sup> through the attack of the adsorbed H atom to the C atom of HCO<sub>3</sub><sup>−</sup> leading to formate formation is much more energetically favoured rather than hydrogenation at its O atoms leading to carboxyl formation.<sup>48</sup> He and Mori's kinetic investigations demonstrate that the attack of the adsorbed H onto the HCO<sub>3</sub><sup>−</sup> species is the rate determining step rather than the dissociation of H<sub>2</sub>.

Here, we report palladium nanoparticles supported on molybdenum carbide, and a synthesis method to produce a more active Pd/Mo<sub>2</sub>C catalyst for the liquid phase hydrogenation of CO<sub>2</sub> to formate, as the reaction solution is in basic conditions. The catalytic activities of four Pd/Mo<sub>2</sub>C monometallic catalysts were studied and compared at mild reaction conditions (100 °C, 2 MPa (CO<sub>2</sub>: H<sub>2</sub> 1:1)), with the most active catalyst producing a significant amount of formate salt with a turnover number (TON) of 109. Palladium is known as an active metal for H<sub>2</sub> activation as well as CO<sub>2</sub> activation,<sup>58</sup> Chen *et al.* reported



Pd/Mo<sub>2</sub>C as the most active catalyst for CO<sub>2</sub> hydrogenation to methanol *albeit* achieving a TON of 4.25, in an environmentally benign solvent (1,4-dioxane), at higher temperatures (135 °C) and pressure (40 bar).<sup>35</sup> Finally, a bimetallic RuPd/Mo<sub>2</sub>C catalyst was also developed and tested for the liquid phase hydrogenation of CO<sub>2</sub>. All monometallic and bimetallic catalysts were tested for their stability and the results were rationalised using a combination of high-resolution transmission electron microscopy (>HR-TEM), field emission gun scanning electron microscopy (FEG-SEM) and density functional theory (DFT) calculations.

## Materials and methods

### Mo<sub>2</sub>C

Two different Mo<sub>2</sub>C materials have been used in this work. Commercial  $\beta$ -Mo<sub>2</sub>C was purchased from Alfa Aesar (99.5% purity) and was used without any further modification.  $\beta$ -Mo<sub>2</sub>C was also synthesized *via* the procedure reported by Volpe *et al.*<sup>59</sup> Briefly,  $\beta$ -Mo<sub>2</sub>C was prepared by the direct carburisation of MoO<sub>3</sub> (0.5 g, B.D.H.) using a flow of 12 ml min<sup>-1</sup> of 20 vol% CH<sub>4</sub> in H<sub>2</sub> (BOC, 99.98%) at 800 °C for 2 hours with a heating rate of 6 °C min<sup>-1</sup> till 350 °C followed by a 1 °C min<sup>-1</sup> heating rate till 800 °C. The resultant material was characterised by powder XRD (ESI,† Fig. S1). Thus prepared  $\beta$ -Mo<sub>2</sub>C was used as support for the synthesis of Pd/Mo<sub>2</sub>C catalyst and was used in the hydrogenation reaction without any further modification.

### M/Mo<sub>2</sub>C synthesis

Two different synthesis methods were used for the preparation of monometallic Pd nanoparticles supported on Mo<sub>2</sub>C (commercial and synthesised) *i.e.* modified wet-impregnation method<sup>60,61</sup> and sol-immobilisation method.<sup>62</sup> Bimetallic RuPd/Mo<sub>2</sub>C was prepared using a modified wet-impregnation method. A brief description of these methods is given below.

### Modified wet-impregnation (MIm) method:

In a typical synthesis, of 2 g of 1 wt% M/Mo<sub>2</sub>C catalyst, the requisite amount of the aqueous metal precursor (metal chloride) solution (equivalent to 0.02 g of metal; in the case of bimetallic catalyst, the two metals were taken in a equimolar ratio) was added to 16 ml of deionized water in a 50 ml glass round bottom flask with vigorous stirring. To this precursor solution, 1.98 g of Mo<sub>2</sub>C was added slowly and steadily with constant stirring at 25 °C. After the completion of the addition of Mo<sub>2</sub>C, the temperature of the stirring slurry was raised to 60 °C and stirred for 30 minutes. Finally, the temperature was raised to 95 °C and left overnight (16 hours) for the complete evaporation of water. After 16 h, the remaining dry, dark-grey solid was ground thoroughly and this dried material was reduced under 5 vol% H<sub>2</sub> in Ar at 400 °C for 4 hours with a heating rate of 10 °C min<sup>-1</sup>. The reduced catalyst was used in the liquid phase reduction of CO<sub>2</sub> without any further modification unless specified otherwise.

### Sol-immobilization (SIm) method

For the synthesis of 1 g of 1 wt% Pd/Mo<sub>2</sub>C catalyst, an aqueous solution of PdCl<sub>2</sub> (Sigma Aldrich) was prepared. Polyvinyl

alcohol (PVA) (1 wt% aqueous solution, Aldrich,  $M_w$  = 10 000, 80% hydrolyzed) and an aqueous solution of NaBH<sub>4</sub> (0.1 M) were also freshly prepared. To the requisite amount of an aqueous solution of PdCl<sub>2</sub>, the required amount of a freshly prepared PVA solution (1 wt%) (PVA/(Au + Pd) (w/w) = 1.3) was added. A freshly prepared solution of NaBH<sub>4</sub> (0.1 M, NaBH<sub>4</sub>/(Pd) (mol/mol) = 5) was then added to form a dark-brown metallic sol. After 30 min of sol-generation, the colloid was immobilized by adding the support material (Mo<sub>2</sub>C (0.99 g) Alfa Aesar). 5 drops of concentrated H<sub>2</sub>SO<sub>4</sub> was added under vigorous stirring. After 2 h, the slurry was filtered, and the catalyst was washed thoroughly with 2 L of distilled water (until the mother liquor was neutral) and then dried at 120 °C overnight under static air in an oven.

All the above-mentioned catalysts were used in the hydrogenation reaction without any further modification or activation.

## Catalyst characterisation

### XRD

The bulk crystalline structures were characterised using X-ray diffraction. Conventional powder X-ray diffraction (PXRD) analysis of the materials was performed on a ( $\theta$ - $\theta$ ) PANalytical X'pert Pro powder diffractometer with a Ni filtered CuK $\alpha$  radiation source operating at 40 keV and 40 mA. Patterns were recorded over the 2 $\theta$  angular range 10–80° using a step size of 0.016°.

### XPS

X-ray photoelectron spectroscopy (XPS) was performed on a Thermo Fisher Scientific K-alpha+ spectrometer. Samples were analysed using a micro-focused monochromatic Al X-ray source (72 W) over an elliptical area of approximately 400  $\mu$ m. Data were recorded at pass energies of 150 eV for survey scans and 40 eV for high resolution scan with 1 eV and 0.1 eV step sizes respectively. Charge neutralisation of the sample was achieved using a combination of both low energy electrons and argon ions. Data analysis was performed in CasaXPS using a Shirley type background and Scofield cross sections, with an energy dependence of –0.6.

### Microscopic studies

Transmission electron microscopy (TEM) were performed on a JEOL JEM-2100 operating at 200 kV. Energy dispersive X-ray analysis (EDX) was done using an Oxford Instruments X-MaxN 80 detector and the data analysed using the Aztec software. Samples were prepared by dispersion in ethanol by sonication and deposited on 300 mesh copper grids coated with holey carbon film. Scanning electron microscopy was performed on a Tescan Maia3 field emission gun scanning electron microscope (FEG-SEM) fitted with an Oxford Instruments X-MaxN 80 energy dispersive X-ray detector (EDX). Images were acquired using the secondary electron and backscattered electron detectors. Samples were prepared by dispersion in ethanol by sonication and deposited on 300 mesh copper grids coated with holey carbon film.



### Catalytic CO<sub>2</sub> hydrogenation reaction and products analyses

The hydrogenation of CO<sub>2</sub> to formate was carried out in a high-pressure stainless steel Parr autoclave (50 ml) reactor fitted with an overhead stirrer. In a typical run, 150 mg of the catalyst was charged into a Teflon liner containing 15 ml of 1 M aqueous NaOH (Sigma Aldrich) solution. Then the Teflon liner was placed inside the autoclave reactor before the reactor was closed airtight. The reactor with its contents was first purged with N<sub>2</sub> (3 times) and then with CO<sub>2</sub> (3 times) to remove traces of air or oxygen from the system and then finally charged with CO<sub>2</sub> (10 bar) and H<sub>2</sub> (10 bar) at 25 °C. Then the reactor was heated to the reaction temperature (100 °C) while stirring at 800 rpm, when the reaction temperature is stabilised, the reaction pressure reaches approximately 26 bar. After 19 h of the reaction time the reactor was cooled to <10 °C using an ice bath, the gas-phase was collected in a gas-bag and the liquid sample was collected and the solid catalyst was removed *via* centrifugation followed by filtration using a syringe filter fitted with a 45 µl filter tip.

The gas phase products were analysed by gas chromatography (Varian 450-GC with a CPSil5 column 50 m × 0.32 mm × 5 µl, fitted with FID), while the liquid products were analysed by high performance liquid chromatography (HPLC) (Agilent 1260 infinity), injected into an Agilent Metacarb 67H column fitted with a refractive index detector. The method ran at 25 °C with a flow rate of 0.25 ml min<sup>-1</sup> with dilute sulfuric acid (0.1 vol%) as the mobile phase. The identity of the products (HCOOH) were confirmed using <sup>1</sup>H-NMR. A series of known standard solutions of formic acid were prepared to generate a calibration curve and response factors, which were used for quantitative analyses of the reaction mixtures.

When stability tests were conducted; 4 identical reactions were run using the procedure above, the solvent was removed by filtration and the catalyst was washed twice with H<sub>2</sub>O and once again with acetone, and left to dry in a vacuum oven. The remaining catalyst was reused using the same reaction procedure as above, washed and dried again to continue the study. The turn over number (TON) was determined as the number of moles of sodium formate produced per mole of metal, calculated using microwave plasma atomic emission spectroscopy (MP-AES) (Agilent 4100), present in the catalyst used. Catalyst was digested in aqua regia first (HCl/HNO<sub>3</sub> = 3 : 1) until all solid was dissolved, before being diluted with water and manually submitted into the instrument.

### Density functional theory calculations

We have modelled the orthorhombic phase of Mo<sub>2</sub>C (*a* = 4.732, *b* = 6.037, *c* = 5.204<sup>63</sup>) and its low Miller-index surfaces. The (001), (010), (011) and (101) surface slabs contained, respectively, 4, 6, 8 and 6 layers of Mo<sub>2</sub>C units, and were separated by a vacuum region of at least 12 Å along the normal to avoid spurious interactions. We performed all geometry optimisations with the VASP 5.3 code,<sup>64,65</sup> using the PBE functional,<sup>66</sup> spin polarisation and the projector augmented wave method,<sup>67</sup> treating explicitly the 5s and 4d electrons of Pd, Ru and Mo, and the 2s and 2p of C.

We adopted a plane wave cut off of 400 eV and scaled the bulk converged 5 × 5 × 5 Monkhorst-Pack<sup>68</sup> grid to 5 × 5 × 1 for surfaces.<sup>69</sup> Optimisations stopped when forces acting on ions were less than 2 × 10<sup>-2</sup> eV Å<sup>-1</sup>.

## Results and discussion

Monometallic Au, Pd and Ru nanoparticles supported on Mo<sub>2</sub>C were prepared *via* the modified wet-impregnation (MIm) method and tested for the CO<sub>2</sub> hydrogenation reaction in liquid phase using an aqueous NaHCO<sub>3</sub> solution as solvent. Results presented in Fig. 1 show that Pd/Mo<sub>2</sub>C unsurprisingly is the most active catalyst for CO<sub>2</sub> hydrogenation, followed by Ru/Mo<sub>2</sub>C and Au/Mo<sub>2</sub>C. Based on this result, Pd/Mo<sub>2</sub>C was used as the catalyst for further tests. It should be noted that Mo<sub>2</sub>C alone managed to produce formate, with no supported metal, confirming that although only a small amount of product was formed (0.0049 mmol), the support material holds catalytic activity. Therefore, when acting as a support for metal nanoparticles, it also acts as a co-catalyst for the reaction.

As discussed in the Introduction section, for CO<sub>2</sub> hydrogenation reactions, an alkaline solution is vital to improve the solubility and reactivity of CO<sub>2</sub> and thereby increase the yield of desired product(s). In order to choose the most appropriate base, the hydrogenation reaction was carried out using different bases (NaHCO<sub>3</sub>, Na<sub>2</sub>CO<sub>3</sub> and NaOH) with and without CO<sub>2</sub>, using 1% Pd/Mo<sub>2</sub>C catalyst at 100 °C for 19 h. Many previous reports in the literature have used NaHCO<sub>3</sub> for CO<sub>2</sub> hydrogenation reaction;<sup>41,45–47</sup> while HCO<sub>3</sub><sup>-</sup> from the sodium bicarbonate is able to form formate in the absence of CO<sub>2</sub>, it has been reported that the presence of CO<sub>2</sub> increases the formate productivity.<sup>70</sup> However, under our reaction conditions more formate was formed from an aqueous NaHCO<sub>3</sub> solution without CO<sub>2</sub> (1.91 mmol) compared to the reaction with CO<sub>2</sub> (1.18 mmol); a decrease of approximately 38% (Fig. 2).

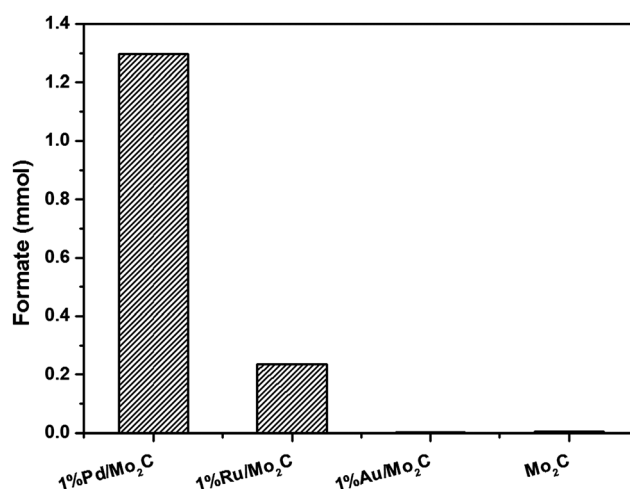


Fig. 1 Screening of different monometallic nanoparticles supported on Mo<sub>2</sub>C for CO<sub>2</sub> hydrogenation reaction. Reaction conditions: 1 wt% M/Mo<sub>2</sub>C; 200 mg (Pd: 0.018 mmol; Ru: 0.019 mmol; Au: 0.01 mmol); stirring speed: 800 rpm; 1 M aqueous NaHCO<sub>3</sub> solution: 20 ml; *p*CO<sub>2</sub>: 10 bar (at 25 °C); *p*H<sub>2</sub>: 10 bar (at 25 °C); reaction temperature: 100 °C; reaction time: 24 h.





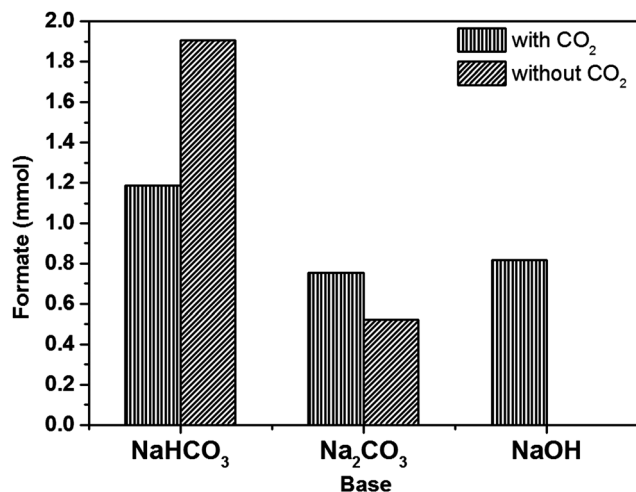


Fig. 2 Production of formate using different bases (NaHCO<sub>3</sub>, Na<sub>2</sub>CO<sub>3</sub> and NaOH) with and without CO<sub>2</sub>. Reaction conditions: 1% Pd/Mo<sub>2</sub>C: 150 mg (Pd: 0.014 mmol); 1 M aqueous base: 15 ml; pCO<sub>2</sub>: 10 bar (25 °C); pH<sub>2</sub>: 10 bar (25 °C) for reaction with CO<sub>2</sub>; pN<sub>2</sub> 10 bar (25 °C) pH<sub>2</sub>: 10 bar (25 °C) only for reaction without CO<sub>2</sub>; reaction temperature: 100 °C; reaction time: 19 h.

This effect may be due to the dissolution of CO<sub>2</sub> affecting the equilibrium of the carbonate species, reducing the amount of HCO<sub>3</sub><sup>−</sup> available in solution for further hydrogenation. Na<sub>2</sub>CO<sub>3</sub> again produces formate in the absence of CO<sub>2</sub>, but more formate was formed in the presence of CO<sub>2</sub> (0.75 mmol) than in the absence of CO<sub>2</sub> (0.52 mmol). When NaOH was used, formate was formed only in the presence of CO<sub>2</sub> (0.82 mmol). When CO<sub>2</sub> was dissolved in 1 M NaOH aqueous reaction mixture, the pH of the solution started decreasing and in 10 min, it stabilized at 8.0 until the end of the reaction. It is well established that at pH 8 the dissolved CO<sub>2</sub> forms HCO<sub>3</sub><sup>−</sup> species, hence it is considered as the intermediate in the formation of formate.<sup>44</sup> During the course of the reaction there is always an equilibrium between CO<sub>2</sub>, HCO<sub>3</sub><sup>−</sup> and HCOO<sup>−</sup>. By choosing NaOH as the base we are confident that the C in HCOO<sup>−</sup> comes from CO<sub>2</sub> only.

The catalytic properties of any supported metal catalyst depend on its structural properties, such as particle size and morphology for monometallic catalysts and additional composition and nanostructure for bimetallic catalysts.<sup>71–75</sup> We have developed a number of synthesis strategies to control these structural properties of monometallic and bimetallic supported Pd catalysts. In an effort to tune the structural properties of the Pd/Mo<sub>2</sub>C catalyst, four different Pd/Mo<sub>2</sub>C structures were synthesised using modified wet-impregnation and sol-immobilisation methods.<sup>60–62</sup> 1% Pd/Mo<sub>2</sub>C and 5% Pd/Mo<sub>2</sub>C were prepared using an aqueous solution of Pd precursor, where PdCl<sub>2</sub> is dissolved in 0.58 M HCl solution; for the purpose of simplicity these will be labelled 1% Pd/Mo<sub>2</sub>C-Mim (0.58 M) and 5% Pd/Mo<sub>2</sub>C-Mim, respectively, for the rest of this paper. Another 1% Pd/Mo<sub>2</sub>C was prepared using another precursor solution where PdCl<sub>2</sub> was dissolved in a 2 M HCl solution, we will label this 1% Pd/Mo<sub>2</sub>C-Mim (2 M). We have reported previously that addition of excess of Cl<sup>−</sup> ions (*via* the addition of either HCl or NaCl) during the wet-impregnation

procedure controls the particle size and morphology of supported AuPd catalysts.<sup>60</sup> Recently Li *et al.* reported the beneficial effect of the addition of excess chloride during the preparation of bimetallic PdRe catalyst for glycerol hydrogenolysis.<sup>76</sup> The fourth catalyst was synthesised using sol-immobilization, which will be labelled 1% Pd/Mo<sub>2</sub>C-SIm. To confirm Mo<sub>2</sub>C was an appropriate support material for this reaction, Pd supported on CeO<sub>2</sub> (1 wt%) was also tested and found that it was almost 20× less active than 1% Pd/Mo<sub>2</sub>C, forming only 0.063 mmol of formate (ESI,† Table S2).

All the four Pd catalysts were tested for CO<sub>2</sub> hydrogenation and the formate yields are presented in the ESI† Table S2. As expected the 1% Pd/Mo<sub>2</sub>C-Mim (2 M), prepared from the precursor in 2 M HCl was found to be much more active (1.53 mmol) in comparison to the 1% Pd/Mo<sub>2</sub>C-Mim (0.58 M) catalyst prepared from 0.58 M HCl (1.09 mmol). However, 5% Pd/Mo<sub>2</sub>C-Mim catalyst gave only 2.14 mmol of formate under the same reaction conditions. For this catalyst, in spite of a 5-fold increase in Pd content compared to 1% Pd/Mo<sub>2</sub>C-Mim (0.58 M) catalyst, the increase in formate yield is less than 2-fold. To normalise the formate productivity with Pd loading, the amounts of Pd present in all these catalysts were determined by MP-AES (ESI,† Table S2), Pd surface content analysis was attempted *via* CO chemisorption, although this proved unsuccessful, possibly due to the low weight loading and low surface area of the large nanoparticles. Actual Pd contents of all the wet-impregnation catalysts were found to be closer to the nominal loading (calculated from the amount of Pd precursor added during the catalyst preparation). The actual loading of the sol-immobilisation catalyst was found to be less than the expected nominal loading, possibly due to inefficient immobilisation of Pd nanoparticles onto the support and their subsequent loss during the washing of 1% Pd/Mo<sub>2</sub>C-SIm catalyst. The TON of all the catalysts, calculated based on the actual amount of Pd (Fig. 3), indicate that 1% Pd/Mo<sub>2</sub>C-Mim (2 M) catalyst prepared from a 2 M HCl solution is

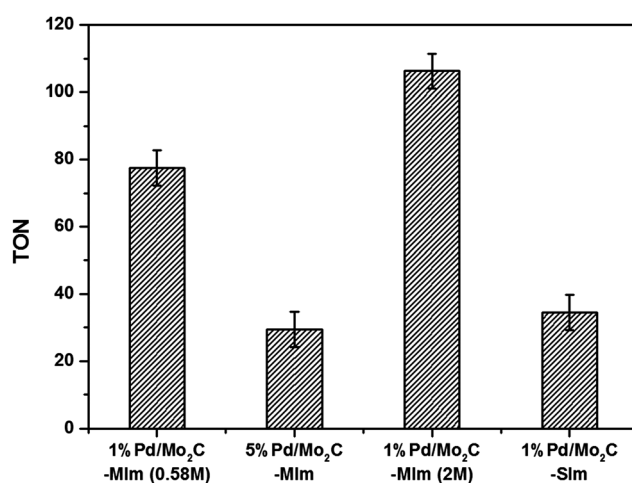


Fig. 3 Comparison of TON for different Pd/Mo<sub>2</sub>C catalysts for the hydrogenation of CO<sub>2</sub> to produce formate. TON is the mol of formate produced per mol of Pd calculated from MP-AES. Reaction condition: Pd/Mo<sub>2</sub>C: 150 mg (1 wt% = 0.014 mmol Pd, 5 wt% = 0.7 mmol Pd); 1 M aqueous NaOH: 15 ml; pCO<sub>2</sub>: 10 bar (at 25 °C); pH<sub>2</sub>: 10 bar (at 25 °C); reaction temperature: 100 °C; reaction time: 19 h.



the most active catalyst exhibiting a TON of 109. Chloride ions have long been considered a poison for noble metal catalysts and chloride precursors have therefore been avoided in the preparation of supported noble metal catalysts. Chen *et al.*, who have previously reported M/Mo<sub>2</sub>C for CO<sub>2</sub> hydrogenation, have avoided the use of PdCl<sub>2</sub> precursor as they report that the chlorine ions poison the catalyst surface and consequently reduce their catalytic activities,<sup>34</sup> which is not the first time Cl<sup>-</sup> ions has considered as a poison.<sup>77,78</sup> However, contradicting reports found Cl<sup>-</sup> ions aid the dispersion of metal nanoparticles on the support surface.<sup>60</sup> Our current results clearly suggest that the addition of an excess of Cl<sup>-</sup> ions, during the preparation of 1% Pd/Mo<sub>2</sub>C-MIm (2 M) catalyst, is beneficial and 1% Pd/Mo<sub>2</sub>C-MIm (2 M) was thus selected for the continuing studies in this paper. We have studied the effect of adding excess of chloride ions during the preparation of Pd based bimetallic catalysts by wet impregnation method in detail.<sup>55,56</sup>

Time on line data (Fig. 4a) for 1% Pd/Mo<sub>2</sub>C-MIm (2 M) catalyst, show that the formation of formate increases steadily with time until 19 h (1.53 mmol of formate) after which time the productivity starts to plateau (1.58 mmol after 24 h). The hydrogenation of CO<sub>2</sub> was also tested at different temperatures (75, 100, 125 and 150 °C) and the formate productivity increases (Fig. 4b) with increasing reaction temperature, which is in line with many reported trends.<sup>79,80</sup> At 75 °C 0.81 mmol of formate was produced and increasing the temperature to 125 °C, we see a remarkable increase in formate productivity, achieving 4.30 mmol of formate, with a TON of 307. At 150 °C formate production increases again to 5.26 mmol. The initial activity (turn over frequency) of 1% Pd/Mo<sub>2</sub>C-MIm (2 M) for the CO<sub>2</sub> hydrogenation at 100 °C is ~14.1 h<sup>-1</sup> during the first initial 2 hours (calculated from ESI†, Fig. S5). It then decreases steadily in an approximately exponential way until it reaches a final activity of 4.6 h<sup>-1</sup> after 19 hours. For a 125 °C reaction we see a TOF of approximately 42.5 h<sup>-1</sup> during the first 2 hours

(Fig. S5, ESI†), and after 19 hours this drops to 16.2 h<sup>-1</sup>. This result is comparable to Mori *et al.*'s Pd/TiO<sub>2</sub> and PdAg/TiO<sub>2</sub> catalysts, achieving TOFs of 12 and 31 h<sup>-1</sup> respectively,<sup>51</sup> also their Ru/LDH catalyst, with TOF of 29. However, this catalyst indeed has a lot of competition and achieves TOFs less than Song *et al.*'s Pd/Chitin (TOF = 257 h<sup>-1</sup>)<sup>42</sup> and Maru *et al.*'s Pd/g-C<sub>3</sub>N<sub>4</sub> (TOF = 660 h<sup>-1</sup>)<sup>81</sup> both achieving results at higher pressure but lower temperatures. A comparison of recent CO<sub>2</sub> hydrogenation catalysts, their TOFs and reaction conditions can be found in the ESI† (Table S1).

The pH of the reaction medium is an important parameter for the dissolution, activation and hence the hydrogenation of CO<sub>2</sub>. As mentioned previously, upon CO<sub>2</sub> dissolution the pH of 1 M NaOH solution (pH = 14) dropped to pH 8 within 10 minutes as bicarbonate species formed in solution. Hence the hydrogenation of CO<sub>2</sub> to formate can be represented as HCO<sub>3</sub><sup>-</sup> + H<sub>2</sub> → HCO<sub>2</sub><sup>-</sup> + H<sub>2</sub>O. Reducing the concentration of NaOH by half (0.5 M), halved the amount of HCOOH formed and the same effect occurred with 0.1 and 0.05 M NaOH solutions (Fig. 5); when no base is added to the reaction solution, the formate production is negligible, resulting in direct correlation between NaOH concentration and formate production.

After optimizing the reaction conditions, we studied the heterogeneous nature of the 1% Pd/Mo<sub>2</sub>C-MIm (2 M) catalyst using the hot filtration method. The catalyst was removed by filtration after 4 h of the reaction (0.6 mmol of formate) and the reaction was continued without any catalyst. There was no increase in the formate yield even after 20 h of further reaction without catalyst (Fig. 6) which proves the heterogeneous nature of the 1% Pd/Mo<sub>2</sub>C-MIm (2 M) catalyst. We further tested the stability and reusability of the Pd/Mo<sub>2</sub>C catalyst by recycling the catalyst two times for CO<sub>2</sub> hydrogenation reactions (Fig. 7a) under identical reaction conditions. The 1% Pd/Mo<sub>2</sub>C-MIm (2 M) catalyst displayed a large drop in the catalytic activity from 1.54 mmol of formate for the fresh catalyst to the

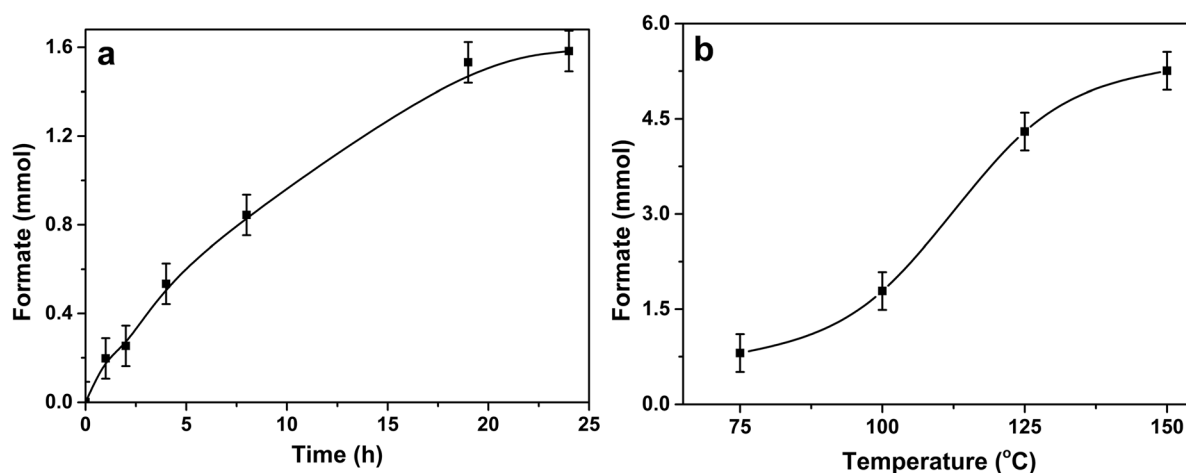


Fig. 4 (a) Time on line evolution of formate over 1% Pd/Mo<sub>2</sub>C catalyst. Reaction condition: 1% Pd/Mo<sub>2</sub>C-MIm (2 M); 150 mg (0.014 mmol Pd); 1 M aqueous NaOH: 15 ml; pCO<sub>2</sub>: 10 bar (at 25 °C); pH<sub>2</sub>: 10 bar (at 25 °C); reaction temperature: 100 °C. (b) Effect of temperature on the production of formate. Reaction condition: 1% Pd/Mo<sub>2</sub>C-MIm (2 M); 150 mg (0.014 mmol Pd); 1 M aqueous NaOH: 15 ml; pCO<sub>2</sub>: 10 bar (at 25 °C); pH<sub>2</sub>: 10 bar (at 25 °C); reaction time: 19 h.



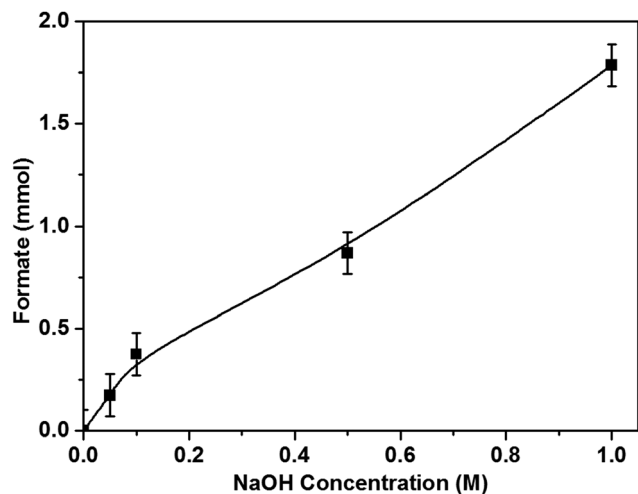


Fig. 5 Effect of NaOH concentration on the production of formate. Reaction conditions: 1% Pd/Mo<sub>2</sub>C-MIm (2 M); 150 mg (0.014 mmol Pd); aqueous alkaline solution of various NaOH concentration: 15 ml; pCO<sub>2</sub>: 10 bar (at 25 °C); pH<sub>2</sub>: 10 bar (at 25 °C); temperature: 100 °C; reaction time: 19 h.

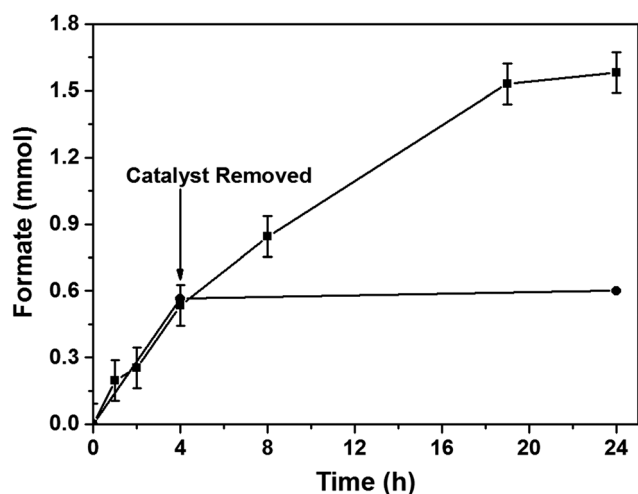


Fig. 6 Catalyst filtration study to show that leaching of Pd is not responsible for the catalytic activity. 1% Pd/Mo<sub>2</sub>C catalyst was filtered after 4 h of the reaction and the reaction was continued with the filtrate until the overall reaction time reaches 24 h (circle). A time-on-line profile of the hydrogenation of CO<sub>2</sub> in the presence of the catalyst is also given for comparison (square). Reaction conditions: 1% Pd/Mo<sub>2</sub>C-MIm (2 M); 150 mg (0.014 mmol Pd); 1 M NaOH: 15 ml; pCO<sub>2</sub>: 10 bar (at 25 °C); pH<sub>2</sub>: 10 bar (at 25 °C); reaction temperature: 100 °C.

0.28 mmol after the 2nd reuse; an 82% drop in the catalytic activity (Fig. 7a).

Commercial Mo<sub>2</sub>C was found to have very low surface area (<1 m<sup>2</sup> g<sup>-1</sup>) as BET and CO chemisorption of Pd/Mo<sub>2</sub>C did not give any reasonable data. It has been reported that synthesised Mo<sub>2</sub>C can have a much higher surface area of 151 m<sup>2</sup> g<sup>-1</sup>.<sup>34</sup> Therefore, increasing the support surface area would be expected to decrease the size of the supported metal nanoparticles and thus improve the catalyst stability. In an effort to improve the stability of the Pd/Mo<sub>2</sub>C catalyst, a fresh batch of β-Mo<sub>2</sub>C was synthesized in the lab. These materials were found to

have a slightly improved surface area of approximately 13 m<sup>2</sup> g<sup>-1</sup> compared to commercial source and was used as the support for the synthesis of 1% Pd/Mo<sub>2</sub>C catalyst. For the purpose of simplicity, this catalyst will be labelled 1% Pd/Mo<sub>2</sub>C-Sy. Another approach to improve catalytic stability was to synthesize a Pd-based bimetallic catalyst. It is well known that the addition of a second metal to Pd can dramatically increase the stability of supported Pd catalysts.<sup>33,82–84</sup> Recently, we reported supported bimetallic RuPd nanoparticles for the hydrodeoxygenation of levulinic acid to γ-valerolactone with enhanced stability.<sup>61,85</sup> Two Pd catalysts were prepared to improve the stability of Pd/Mo<sub>2</sub>C catalyst based on the two approaches mentioned above. 1% Pd/Mo<sub>2</sub>C-Sy was prepared using home-made β-Mo<sub>2</sub>C and a bimetallic 1% RuPd/Mo<sub>2</sub>C (commercially sourced Mo<sub>2</sub>C) and both these catalysts were tested for catalytic activity and stability. Lab-synthesised β-Mo<sub>2</sub>C support neither improved the catalytic activity nor the stability of 1% Pd/Mo<sub>2</sub>C (Fig. 7d). However, the bimetallic 1% RuPd/Mo<sub>2</sub>C displayed a much better stability compared to the monometallic 1% Pd/Mo<sub>2</sub>C-MIm (2 M) catalyst, we did not load the lab synthesised β-Mo<sub>2</sub>C with RuPd bimetallic nanoparticles as the commercial and synthesised supports produced the similar results when loaded with Pd monometallic nanoparticles. For the monometallic catalyst, during the 2nd reuse, an 82% reduction in activity was observed, whereas for the bimetallic RuPd catalyst only a 30% drop in activity was observed (Fig. 7c). The total Pd contents of fresh and spent catalysts were analysed by MP-AES (ESI,† Table S3), which showed that there is no decrease in Pd content, suggesting there is no leaching of Pd which was further confirmed by the absence of Pd in the reaction mixture.

In an effort to understand the reason for this deactivation, the Pd metal particle size of fresh and used catalysts, all fresh and used catalysts were analysed by HR-TEM and FEG-SEM. When observing catalysts synthesised using a commercially sourced Mo<sub>2</sub>C, HR-TEM image (Fig. 8a), showed large, highly crystalline Mo<sub>2</sub>C particles, which implies that the support has a very small surface area and few defects on the surface for Pd nanoparticles to bind to, resulting in large Pd particles on the surface. Due to the density of the Mo<sub>2</sub>C support, the HR-TEM images give us minimal information as the material was blocking any transmission through the bulk of the material. FEG-SEM provides us with more detail with respect to the size of the metal particles and the nature of the support surface. The LE-BSE detector was used for distinguishing the palladium from the molybdenum surface. The BSE is strongly related to atomic number, with heavier elements backscattering more electrons, thereby contributing to a brighter signal. Large Pd nanoparticles can be observed (Fig. 8b) with a size range of approximately 50–70 nm and a good dispersion. When analysing the elemental composition of the Mo<sub>2</sub>C surface, EDX showed a Pd wt% of 0.5–0.8%, which is a good result for a 1 wt% loading. Characterising the used Pd/Mo<sub>2</sub>C sample we see a less even particle distribution and large agglomerations of palladium particles with sizes of approx. 1 μm (Fig. 8c), phase separated agglomerations were also found isolated from the support (not shown). This implies that during reaction, due to a weak



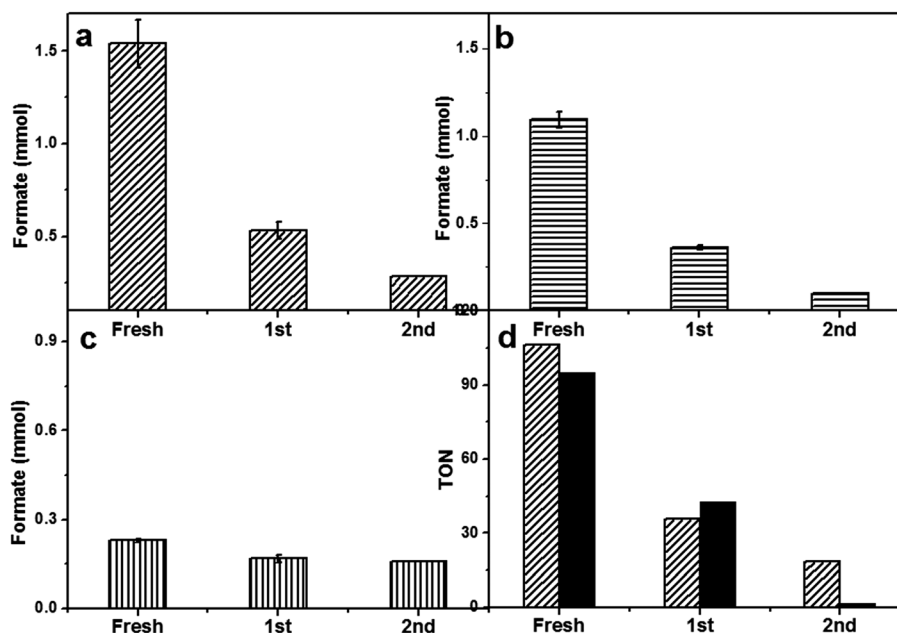


**Fig. 7** Stability studies of Pd/Mo<sub>2</sub>C and RuPd/Mo<sub>2</sub>C catalysts. All catalysts were reused 2×. (a) Formate formed with 1% Pd/Mo<sub>2</sub>C-MIm (2 M), (b) formate formed with Pd/Mo<sub>2</sub>C-MIm (0.58 M), (c) formate formed with 1% RuPd/Mo<sub>2</sub>C, (d) TON of formate production from 1% Pd/Mo<sub>2</sub>C-MIm (2 M) with commercially sourced Mo<sub>2</sub>C (patterned bar) and 1% Pd/Mo<sub>2</sub>C-Sy with lab synthesised Mo<sub>2</sub>C (solid bar). Reaction conditions (a – c + d (patterned bar)): M/Mo<sub>2</sub>C: 150 mg (monometallic: 0.014 mmol Pd) (bimetallic 0.007 mmol (Pd,Ru)); 1 M NaOH: 15 ml; pCO<sub>2</sub>: 10 bar (at 25 °C); pH<sub>2</sub>: 10 bar (at 25 °C); temperature: 100 °C; reaction time: 19 h. Reaction conditions (d (solid bar)): 10 ml stainless steel autoclave: M/Mo<sub>2</sub>C: 40 mg; 1 M NaOH: 4 ml; pCO<sub>2</sub>: 10 bar (at 25 °C); pH<sub>2</sub>: 10 bar (at 25 °C); reaction temperature: 100 °C; reaction time: 19 h.

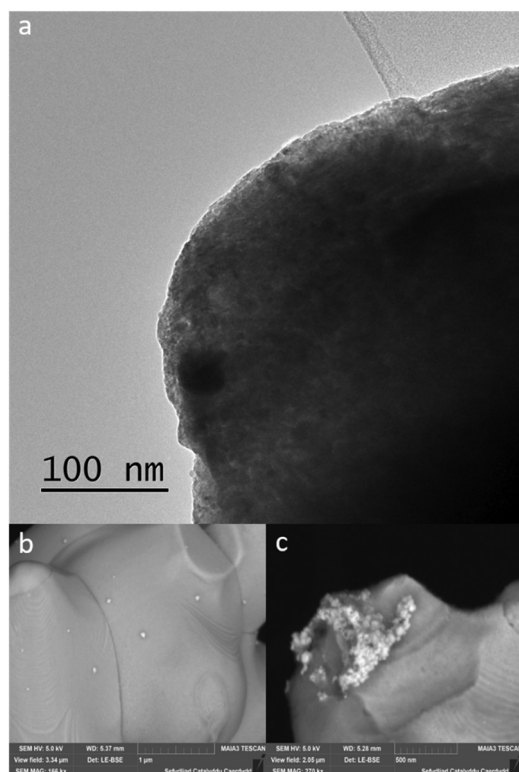


**Fig. 8** (a) HR-TEM images of fresh 1% Pd/Mo<sub>2</sub>C-MIm (2 M). FEG-SEM images of (b) fresh 1% Pd/Mo<sub>2</sub>C-MIm (2 M) LE-BSE (c) used 1% Pd/Mo<sub>2</sub>C-MIm (2 M), Pd cluster LE-BSE.

metal-support interaction and surface decomposition, palladium nanoparticles sinter, and in turn, are lost from the support as heterogeneous particles, explaining the drop in catalytic activity. This did not show in the leaching studies as the particles are too large to be retained in the filtrate solution. Tests were run to confirm that these Pd particles were not the catalyst for formate production; PdCl<sub>2</sub> and Pd colloids were catalytically tested and compared to 1% Pd/Mo<sub>2</sub>C-MIm (2 M), using the same palladium weight and reaction conditions. Formate productivities of 0.06 and 0.09 mmol were observed for PdCl<sub>2</sub> solution and Pd colloids respectively (ESI,† Fig. S2), compared to 0.42 mmol produced from 1% Pd/Mo<sub>2</sub>C-MIm (2 M). This confirms that the metal-support interactions are indeed causing an increase in catalytic activity of the palladium. Observing fresh bimetallic 1% RuPd/Mo<sub>2</sub>C under HR-TEM and FEG-SEM shows a larger range of metal nanoparticle sizes, ca. 10–85 nm, with an even dispersion over the support (Fig. 9a). Analysing recycled 1% RuPd/Mo<sub>2</sub>C, it was found that the metal particles had increased in size (Fig. 9c), exceeding 100 nm. However, no metal particles, palladium or ruthenium, were found isolated from the support. This implies that, although there was sintering along the support surface during reaction, the addition of the ruthenium creates a stronger metal-support interaction and as a result, no metal particles are lost from the support, explaining the improved stability compared to the monometallic 1% Pd/Mo<sub>2</sub>C.

We have used atomistic simulations based on DFT to shed light on the improved stability of the bimetallic nanoparticles. In order to have a model for the support, we have first calculated the surface energies,  $\gamma$ , of the low index (001), (010), (011) and



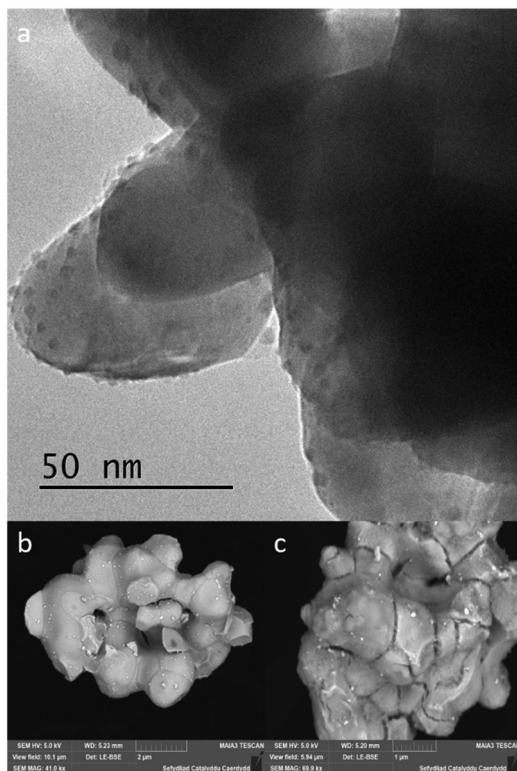


Fig. 9 (a) HR-TEM image of fresh 1% RuPd/Mo<sub>2</sub>C; FEG-SEM images: (b) fresh 1% RuPd/Mo<sub>2</sub>C LE-BSE, (c) used 1% RuPd/Mo<sub>2</sub>C LE-BSE.

(101) surfaces of orthorhombic Mo<sub>2</sub>C, shown in ESI,<sup>†</sup> Fig. S3, according to the formula:

$$\gamma = \frac{1}{2A}(E_{\text{slab}} - NE_{\text{Mo}_2\text{C}}), \quad (1)$$

where  $E_{\text{slab}}$  is the energy of the slab with surface area  $A$  and containing  $N$  Mo<sub>2</sub>C units,  $E_{\text{Mo}_2\text{C}}$  is the energy per formula unit of bulk Mo<sub>2</sub>C, and the factor 2 takes into account the two symmetric terminations of the surface slabs. Note that we have not considered the polar (100), (110) and (111) surfaces as they would undergo a significant reconstruction to eliminate the electric dipole moment<sup>86</sup> and are generally less stable.<sup>29</sup>

We report in ESI,<sup>†</sup> Table S4 the surface energies of the different surfaces. Our calculations indicate that the (101) is the most stable face of Mo<sub>2</sub>C, in agreement with the previous literature,<sup>87</sup> followed by the (010), (011) and (001). In view of these results, we have used the (101) and (010) surfaces as substrate models for the adsorption of single Pd and Ru atoms.

Fig. 10 illustrates the adsorption sites obtained after relaxing a number of different initial positions. On the (101) surface, *a* and *b* are sixfold hollow sites. Here, the metal adatoms coordinate to one C and four Mo atoms of the top layer, in addition to one Mo atom of the second layer. In *c*, which is a fourfold hollow site, the adatoms coordinate only to topmost Mo atoms. Site *d* is threefold, and the adatoms form a bridging bond with two Mo besides bonding a third C atom. Considering the (010) surface, site *e* is above a C atom of the topmost layer, while *f* is a sixfold hollow site. Finally, *g* and *h* are different bridging sites.

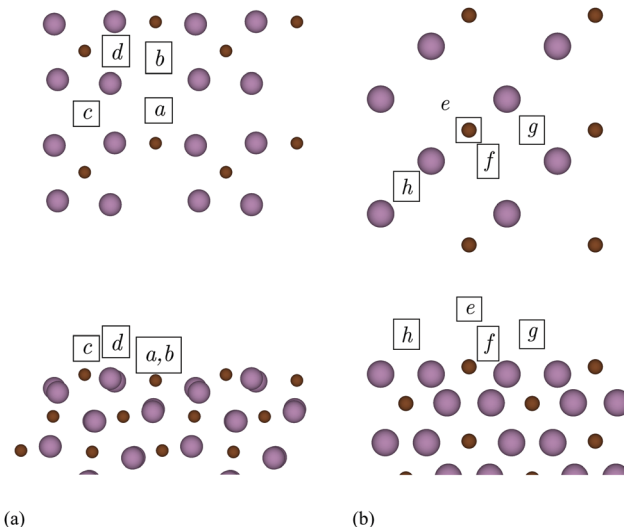


Fig. 10 Adsorption sites on the (101) (a) and (010) (b) surfaces of Mo<sub>2</sub>C. Top and bottom panels show top and side views, respectively. Only the atoms of the topmost Mo<sub>2</sub>C layers are depicted in the top views. Colour code: Mo – large purple spheres, C – small brown spheres.

Table 1 Adsorption energies at the different sites of the (101) and (010) surfaces of Mo<sub>2</sub>C. Site labels refer to Fig. 10

Surface	Site	$\Delta E$ (eV per atom)	
		Pd	Ru
(101)	a	−4.25	−6.52
	b	−4.03	−6.17
	c	−4.34	−6.05
	d	−3.06	−4.77
(010)	e	−3.01	−4.35
	f	−3.05	−4.54
	g	−4.19	−6.40
	h	−3.71	−5.36

We list in Table 1 the adsorption energies,  $\Delta E$ , of Pd and Ru atoms at the sites described above, which have been calculated according to the formula:

$$\Delta E = \frac{1}{2}(E_{2M/\text{slab}} - E_{\text{slab}} - 2E_M), \quad (2)$$

where  $E_{2M/\text{slab}}$  and  $E_{\text{slab}}$  are the energies of the slab with and without the metal adatoms  $M$ ,  $E_M$  is the energy of  $M$  in the gas phase and the factor 2 takes into account the fact that adsorptions occur on symmetric terminations. For all sites of both surfaces,  $\Delta E$  is more negative for Ru compared to Pd, with a difference which ranges from 1.3 to 2.3 eV. These results represent evidence that Ru atoms have significantly better affinities than Pd to the Mo<sub>2</sub>C support adopted in the experiment. We propose that the Ru atoms act like a link between Pd and the Mo<sub>2</sub>C support and thereby increase the stability and reusability of the bimetallic RuPd catalyst.

Pd/Mo<sub>2</sub>C and RuPd/Mo<sub>2</sub>C catalysts were characterised by XPS. From previous XPS studies of Mo<sub>2</sub>C catalysts, Moon *et al.* concluded that the deactivation of a Mo<sub>2</sub>C catalyst is caused by the transformation of Mo<sub>2</sub>C (Mo<sup>2+</sup>) to MoO<sub>3</sub> (Mo<sup>6+</sup>) on the



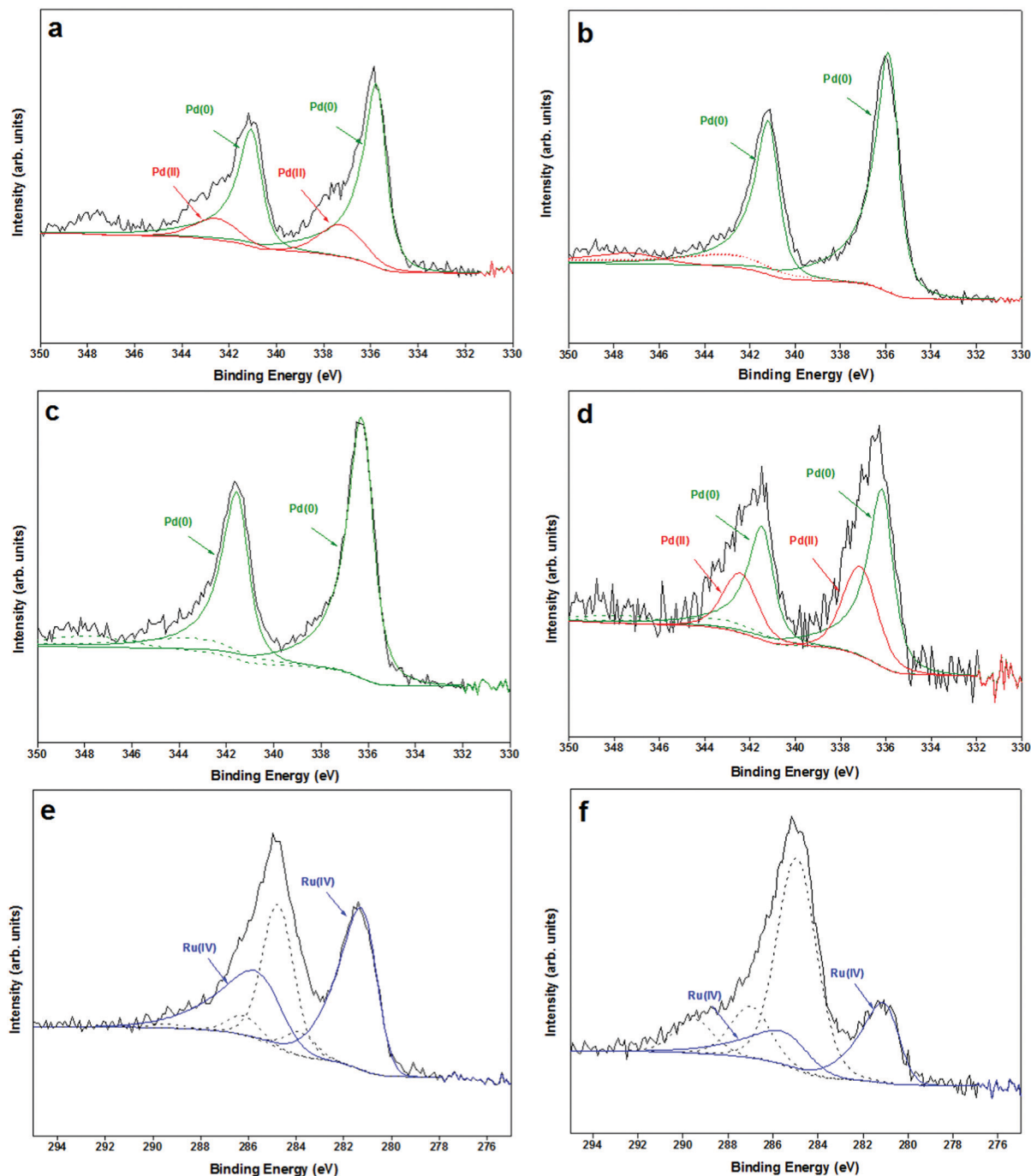


Fig. 11 Pd 3d XPS spectra of 1% Pd/Mo<sub>2</sub>C-MIm (2 M) (a) fresh sample (b) 3× used sample, and 1% RuPd/Mo<sub>2</sub>C (c) fresh sample (d) 3× used sample; displaying Pd(0) (green) and Pd(II) (red). Ru 3d XPS spectra of 1% RuPd/Mo<sub>2</sub>C (e) fresh sample (f) 3× used sample, displaying RuO<sub>2</sub> (blue) species.

surface of the catalyst in the presence of H<sub>2</sub>O during WGS reaction.<sup>88</sup> X-ray photoelectron spectroscopic data (Mo 3d) of 1% Pd/Mo<sub>2</sub>C-MIm (2 M) (ESI,† Fig. S4) reveals that the support is predominantly oxidised with several oxidation states of molybdenum ranging from Mo<sup>(δ+)</sup> to Mo<sup>(6+)</sup> ( $1 < \delta < 4$ ). However, these oxidised species do not show much deviation between the fresh and used samples. In respect of the metal, palladium is observed as a well resolved doublet, with the Pd3d<sub>5/2</sub> centred at 335.7 eV, and exhibiting shake-up structure

to higher binding energies indicative of metallic Pd<sup>56</sup> and Pd3d<sub>5/2</sub> centred at 337 eV indicative of Pd(II) (Fig. 11). Post-reaction we only see Pd(0) present in the sample possibly accounting to the hydrogenation conditions of the reaction process.

In the XPS of bimetallic RuPd samples, Ru peak (Fig. 11) is observed as an asymmetric doublet with Ru3d<sub>5/2</sub> centred at ca. 281 eV indicative of RuO<sub>2</sub>.<sup>89</sup> The amount of Pd(II) increases post-reaction (Fig. 11d) which may be a result of some charge transfer from Pd to Ru. This is in line with Zhang *et al.*, who reported that



**Table 2** Binding energies (eV) and curve-fitting results of Pd and Ru 3d XPS spectra

Sample	Pd(0)		Pd(II)		Ru(IV)	
	3d <sub>5/2</sub> , eV	3d <sub>3/2</sub> , eV	3d <sub>5/2</sub> , eV	3d <sub>3/2</sub> , eV	3d <sub>5/2</sub> , eV	3d <sub>3/2</sub> , eV
1% Pd/Mo <sub>2</sub> C-MIm (2 M) fresh	335.73	341.03	337.25	342.55	—	—
1% Pd/Mo <sub>2</sub> C-MIm (2 M) used	335.84	341.14	—	—	—	—
1% RuPd/Mo <sub>2</sub> C fresh	336.20	341.50	—	—	281.03	285.23
1% RuPd/Mo <sub>2</sub> C used	336.11	341.41	337.06	342.36	280.71	284.91

for PdRu bimetallic samples the addition of Ru increases Pd(II) species.<sup>90</sup> Ru(IV) has a higher reduction potential (+1.12  $E^\circ/V$ ) than Pd(II) (+0.95  $E^\circ/V$ ) causing an electron transfer from Pd to Ru resulting in an increase in Pd(II) species, which could be one of the reasons for the deactivation of this bimetallic catalyst.

A positive shift (+0.5 eV) of the Pd 3d binding energies is observed for the RuPd bimetallic catalyst compared to the monometallic Pd catalyst (Table 2), indicating that a change in the electronic properties of Pd is modified upon alloying with Ru.<sup>90</sup> Comparing the fresh and used RuPd bimetallic catalyst, shifts for the Pd 3d binding energies are within experimental error, however a negative shift (−0.3 eV) for the Ru 3d binding energy in the post reaction catalyst is observed, suggesting that there are still some alloy properties even after 3 uses, but it has decreased. It is this alloying affect that may be the reason of the bimetallic increased stability, as this metal–metal interaction is contributing to stronger metal–support interaction for Pd. Unfortunately, due to the similar atomic number of Pd, Ru and Mo it has proved very difficult to confirm this alloying through EDX.

The initial rate of formation of formate were calculated at different temperatures (75, 100 & 125 °C) for both monometallic Pd/Mo<sub>2</sub>C and bimetallic RuPd/Mo<sub>2</sub>C catalysts under standard conditions for the first 2 hours of the reaction (ESI<sup>†</sup>, Fig. S5 + S6). Using this rate data, the apparent activation energies for 1% Pd/Mo<sub>2</sub>C and 1% RuPd/Mo<sub>2</sub>C were calculated as +36 kJ mol<sup>−1</sup> and +43 kJ mol<sup>−1</sup> respectively. Luo *et al.*<sup>61</sup> reported that alloying RuPd results in Ru diluting and isolating certain active sites of Pd, which may result in this increase in activation energy as well as creating stabilising effects. In comparison with the literature, these results are lower than Chen *et al.*'s work, reporting CO<sub>2</sub> hydrogenation to methanol Fe and Cu supported on Mo<sub>2</sub>C within an organic solvent, with activation energies of +96 and +105 kJ mol<sup>−1</sup> respectively.<sup>34</sup> In other catalytic systems known for hydrogenation of CO<sub>2</sub> and HCO<sub>3</sub><sup>−</sup> salts, the activation energy values are larger than our Pd/Mo<sub>2</sub>C catalyst, for example +54.3 kJ mol<sup>−1</sup> for Ru/LDH,<sup>41</sup> +39 kJ mol<sup>−1</sup> with Pd/C catalyst.<sup>91,92</sup> The activation energy is similar to certain homogeneous catalysts [RhCl(TPPMS)<sub>3</sub>]<sup>93</sup> with +36 kJ mol<sup>−1</sup>. But higher than others for example with K[RuCl(EDTA-H)]<sup>94</sup> it is +31 kJ mol<sup>−1</sup>, and [RhCl(TPPTS)<sub>3</sub>]<sup>95</sup> it is 25 kJ mol<sup>−1</sup>.

## Conclusions

Here we report 1% Pd/Mo<sub>2</sub>C as an active catalyst for the liquid phase hydrogenation of CO<sub>2</sub> to formate under relatively mild reaction conditions. It was found that increasing the HCl

concentration from 0.58 M to 2 M for the preparation of PdCl<sub>2</sub> precursor solution for catalyst preparation increased the catalytic activity by more than 70%, producing 1.5 mmol of formate with a TON of 109 and activation energy of +36 kJ. Our study found that compared to NaHCO<sub>3</sub> and Na<sub>2</sub>CO<sub>3</sub>, a 1 M NaOH basic solvent proved the most effective as it allowed 100% of formate formed to be derived from the CO<sub>2</sub>. Stability studies and electron microscopy data found that 1% Pd/Mo<sub>2</sub>C has a poor reusability as Pd nanoparticles easily sinter and can be partially lost from the support. However, when introducing ruthenium in a bimetallic 1% RuPd/Mo<sub>2</sub>C catalyst, although less active, greatly improves its reusability. Simulations based on DFT have found that the adsorption energies of Ru on the Mo<sub>2</sub>C surfaces are significantly lower than Pd. As such, Ru atoms have a stronger affinity towards the Mo<sub>2</sub>C support. XPS data suggests close interaction between Pd and Ru, thus, in the bimetallic catalyst the Ru atoms act like a link between the Pd and Mo<sub>2</sub>C surface, resulting in an increased stability of the RuPd/Mo<sub>2</sub>C catalyst.

## Conflicts of interest

There are no conflicts of interest to declare.

## Acknowledgements

We thank the Cardiff University electron microscopy facility for the transmission (TEM) and scanning electron microscopy (SEM). XPS data collection was performed at the EPSRC National Facility for XPS ('HarwellXPS'), operated by Cardiff University and UCL, under contract No. PR16195. Via our membership of the UK's HEC Materials Chemistry Consortium, which is funded by EPSRC (EP/L000202), this work used the ARCHER UK National Supercomputing Service (<http://www.archer.ac.uk>). All data created during this research are openly available from the Cardiff University Research Portal at <http://doi.org/10.6084/m9.figshare.9586913>.

## References

- 1 R. Kawase, Y. Matsuoka and J. Fujino, *Energy Policy*, 2006, **34**, 2113–2122.
- 2 P. Nejat, F. Jomehzadeh, M. M. Taheri, M. Gohari and M. Z. Abd. Majid, *Renewable Sustainable Energy Rev.*, 2015, **43**, 843–862.
- 3 G. Centi and S. Perathoner, *Catal. Today*, 2009, **148**, 191–205.
- 4 G. Centi, E. A. Quadrelli and S. Perathoner, *Energy Environ. Sci.*, 2013, **6**, 1711.



- 5 A. Dibenedetto, A. Angelini and P. Stufano, *J. Chem. Technol. Biotechnol.*, 2014, **89**, 334–353.
- 6 E. A. Quadrelli, G. Centi, J.-L. Duplan and S. Perathoner, *ChemSusChem*, 2011, **4**, 1194–1215.
- 7 Unfccc, Adoption of the Paris Agreement – Paris Agreement text English.
- 8 P. Styring, D. Jansen, H. de Coninck, H. Reith and K. Armstrong, Carbon Capture and Utilisation in the green economy, 2011.
- 9 S. Ghazali-Esfahani, H. Song, E. Păunescu, F. D. Bobbink, H. Liu, Z. Fei, G. Laurenczy, M. Bagherzadeh, N. Yan and P. J. Dyson, *Green Chem.*, 2013, **15**, 1584.
- 10 E. Alper and O. Yuksel Orhan, *Petroleum*, 2017, **3**, 109–126.
- 11 S. Y. Tee, K. Y. Win, W. S. Teo, L.-D. Koh, S. Liu, C. P. Teng and M.-Y. Han, *Adv. Sci.*, 2017, **4**, 1600337.
- 12 M. Ni, M. K. H. Leung, D. Y. C. Leung and K. Sumathy, *Renewable Sustainable Energy Rev.*, 2007, **11**, 401–425.
- 13 J. Eppinger and K.-W. Huang, *ACS Energy Lett.*, 2017, **2**, 188–195.
- 14 A. Weilhard, M. I. Qadir, V. Sans and J. Dupont, *ACS Catal.*, 2018, **8**, 1628–1634.
- 15 G. Peng, S. J. Sibener, G. C. Schatz and M. Mavrikakis, *Surf. Sci.*, 2012, **606**, 1050–1055.
- 16 T. Maihom, S. Wannakao, B. Boekfa and J. Limtrakul, *J. Phys. Chem. C*, 2013, **117**, 17650–17658.
- 17 D. Mellmann, P. Sponholz, H. Junge and M. Beller, *Chem. Soc. Rev.*, 2016, **45**, 3954–3988.
- 18 J. Klankermayer, S. Wesselbaum, K. Beydoun and W. Leitner, *Angew. Chem., Int. Ed.*, 2016, **55**, 7296–7343.
- 19 S. A. Burgess, K. Grubel, A. M. Appel, E. S. Wiedner and J. C. Linehan, *Inorg. Chem.*, 2017, **56**, 8580–8589.
- 20 M. Rumayor, A. Dominguez-Ramos and A. Irabien, *Appl. Sci.*, 2018, **8**, 914.
- 21 S. Moret, P. J. Dyson and G. Laurenczy, *Nat. Commun.*, 2014, **5**, 4017.
- 22 R. Tanaka, M. Yamashita and K. Nozaki, *J. Am. Chem. Soc.*, 2009, **131**, 14168–14169.
- 23 H. Hayashi, S. Ogo and S. Fukuzumi, *Chem. Commun.*, 2004, 2714–2715.
- 24 C. Ziebart, C. Federsel, P. Anbarasan, R. Jackstell, W. Baumann, A. Spannenberg and M. Beller, *J. Am. Chem. Soc.*, 2012, **134**, 20701–20704.
- 25 E. T. Liakakou and E. Heracleous, *Catal. Rev. Eng.*, 2016, **6**, 1106–1119.
- 26 N. M. Schweitzer, J. A. Schaidle, O. K. Ezekoye, X. Pan, S. Linic and L. T. Thompson, *J. Am. Chem. Soc.*, 2011, **133**, 2378–2381.
- 27 B. Dhandapani, T. St. Clair and S. T. Oyama, *Appl. Catal., A*, 1998, **168**, 219–228.
- 28 P. Liang, H. Gao, Z. Yao, R. Jia, Y. Shi, Y. Sun, Q. Fan and H. Wang, *Catal. Sci. Technol.*, 2017, **7**, 3312–3324.
- 29 M. G. Quesne, A. Roldan, N. H. de Leeuw and C. R. A. Catlow, *Phys. Chem. Chem. Phys.*, 2018, **20**, 6905–6916.
- 30 J.-L. Dubois, K. Sayama and H. Arakawa, *Chem. Lett.*, 1992, 5–8.
- 31 A. B. Vidal, L. FERIA, J. Evans, Y. Takahashi, P. Liu, K. Nakamura, F. Illas and J. A. Rodriguez, *J. Phys. Chem. Lett.*, 2012, **3**, 2275–2280.
- 32 L. Fan, Y. Sakaiya and K. Fujimoto, *Appl. Catal., A*, 1999, **180**, L11–L13.
- 33 A. García-Trenco, A. Regoutz, E. R. White, D. J. Payne, M. S. P. Shaffer and C. K. Williams, *Appl. Catal., B*, 2018, **220**, 9–18.
- 34 Y. Chen, S. Choi and L. T. Thompson, *J. Catal.*, 2016, **343**, 147–156.
- 35 Y. Chen, S. Choi and L. T. Thompson, *ACS Catal.*, 2015, **5**, 1717–1725.
- 36 S. D. Richardson and S. Y. Kimura, *Environ. Technol. Innov.*, 2017, **8**, 40–56.
- 37 I. U. Din, M. S. Shaharun, A. Naeem, S. Tasleem and M. Rafie Johan, *Chem. Eng. J.*, 2018, **334**, 619–629.
- 38 P. G. Jessop, Y. Hsiao, T. Ikariya and R. Noyori, *J. Am. Chem. Soc.*, 1996, **118**, 344–355.
- 39 C. Yin, Z. Xu, S.-Y. Yang, S. Man Ng, K. Yin Wong, Z. Lin and C. Po Lau, *Organometallics*, 2001, **20**, 1216–1222.
- 40 S. Posada-Perez, *Phys. Chem. Chem. Phys.*, 2014, **16**, 14912–14921.
- 41 K. Mori, T. Taga and H. Yamashita, *ACS Catal.*, 2017, **7**, 3147–3151.
- 42 H. Song, N. Zhang, C. Zhong, Z. Liu, M. Xiao and H. Gai, *New J. Chem.*, 2017, **41**, 9170–9177.
- 43 Z. Duan and R. Sun, *Chem. Geol.*, 2003, **193**, 257–271.
- 44 O. Pedersen, T. D. Colmer and K. Sand-Jensen, *Front. Plant Sci.*, 2013, **4**, 140.
- 45 Y. M. Badiei, W.-H. Wang, J. F. Hull, D. J. Szalda, J. T. Muckerman, Y. Himeda and E. Fujita, *Inorg. Chem.*, 2013, **52**, 12576–12586.
- 46 E. Fujita and Y. Himeda, *Biochim. Biophys. Acta, Bioenerg.*, 2013, **1827**, 1031–1038.
- 47 L. Gábor, J. Ferenc and L. Nádasd, *Inorg. Chem.*, 2000, **39**, 5083–5088.
- 48 G. Peng, S. J. Sibener, G. C. Schatz, S. T. Ceyer and M. Mavrikakis, *J. Phys. Chem. C*, 2012, **116**, 3001–3006.
- 49 F. Wang, J. Xu, X. Shao, X. Su, Y. Huang and T. Zhang, *ChemSusChem*, 2016, **9**, 246–251.
- 50 C. S. He, L. Gong, J. Zhang, P. P. He and Y. Mu, *J. CO<sub>2</sub> Util.*, 2017, **19**, 157–164.
- 51 K. Mori, T. Sano, H. Kobayashi and H. Yamashita, *J. Am. Chem. Soc.*, 2018, **140**, 8902–8909.
- 52 W.-H. Wang, Y. Himeda, J. T. Muckerman, G. F. Manbeck and E. Fujita, *Chem. Rev.*, 2015, **115**, 12936–12973.
- 53 H. Conrad, G. Ertl and E. E. Latta, *Surf. Sci.*, 1974, **41**, 435–446.
- 54 I. Cabria, M. J. López López, S. Fraile and J. A. Alonso, *J. Phys. Chem. C*, 2012, **116**, 21179–21189.
- 55 T. Mitsui, M. K. Rose, E. Fomin, D. F. Ogletree and M. Salmeron, *Nature*, 2003, **422**, 705–707.
- 56 X. Wang, N. Perret, L. Delannoy, C. Louis and M. A. Keane, *Catal. Sci. Technol.*, 2016, **6**, 6932–6941.
- 57 S. Posada-Pérez, F. Viñes, R. Valero, J. A. Rodriguez and F. Illas, *Surf. Sci.*, 2017, **656**, 24–32.
- 58 W. Wang, S. Wang, X. Ma and J. Gong, *Chem. Soc. Rev.*, 2011, **40**, 3703.
- 59 L. Volpe and M. Boudart, *J. Solid State Chem.*, 1985, **59**, 348–356.
- 60 M. Sankar, Q. He, M. Morad, J. Pritchard, S. J. Freakley, J. K. Edwards, S. H. Taylor, D. J. Morgan, A. F. Carley,





- D. W. Knight, C. J. Kiely and G. J. Hutchings, *ACS Nano*, 2012, **6**, 6600–6613.
- 61 W. Luo, M. Sankar, A. M. Beale, Q. He, C. J. Kiely, P. C. A. Bruijninx and B. M. Weckhuysen, *Nat. Commun.*, 2015, **6**, 1–10.
- 62 N. Dimitratos, A. Villa and L. Prati, *Catal. Lett.*, 2009, **133**, 334–340.
- 63 A. N. Christensen, *Acta Chem. Scand., Ser. A*, 1997, **31**, 509–511.
- 64 G. Kresse and J. Hafner, *Phys. Rev. B: Condens. Matter Mater. Phys.*, 1993, **47**, 558–561.
- 65 G. Kresse and J. Furthmuller, *J. Comput. Mater. Sci.*, 1996, **6**, 15–50.
- 66 J. P. Perdew, K. Burke and M. Ernzerhof, *Phys. Rev. Lett.*, 1996, **77**, 3865.
- 67 P. E. Blöchl, *Phys. Rev. B: Condens. Matter Mater. Phys.*, 1994, **50**, 17953.
- 68 H. J. Monkhorst and J. D. Pack, *Phys. Rev. B: Solid State*, 1976, **13**, 5188.
- 69 J. R. D. S. Politi, F. Vines, J. A. Roriguez and F. Illas, *Phys. Chem.*, 2013, **15**, 12617–12625.
- 70 K. Rohmann, J. Kothe, M. W. Haenel, U. Englert, M. Hölscher and W. Leitner, *Angew. Chem., Int. Ed.*, 2016, **55**, 8966–8969.
- 71 G. J. Hutchings and C. J. Kiely, *Acc. Chem. Res.*, 2013, **46**, 1759–1772.
- 72 D. Wu, K. Kusada and H. Kitagawa, *Sci. Technol. Adv. Mater.*, 2016, **17**, 583–596.
- 73 J. Yang, C. Tian, L. Wang and H. Fu, *J. Mater. Chem.*, 2011, **21**, 3384.
- 74 M. L. Toebe, J. A. van Dillen and K. P. de Jong, *J. Mol. Catal. A: Chem.*, 2001, **173**, 75–98.
- 75 P. Paalanen, B. M. Weckhuysen and M. Sankar, *Catal. Sci. Technol.*, 2013, **3**, 2869.
- 76 Y. Li, H. Liu, L. Ma and D. He, *Appl. Catal., A*, 2016, **522**, 13–20.
- 77 T. Narita, H. Miura, M. Ohira, H. Hondou, K. Sugiyama, T. Matsuda and R. D. Gonzalez, *Appl. Catal.*, 1987, **32**, 185–190.
- 78 V. Ragaini, R. Carli, C. L. Bianchi, D. Lorenzetti and G. Vergani, *Appl. Catal., A*, 1996, **139**, 17–29.
- 79 L. T. M. Nguyen, H. Park, M. Banu, J. Y. Kim, D. H. Youn, G. Magesh, W. Y. Kim and J. S. Lee, *RSC Adv.*, 2015, **5**, 105560–105566.
- 80 D. Preti, C. Resta, S. Squarcialupi and G. Fachinetti, *Angew. Chem., Int. Ed.*, 2011, **50**, 12551–12554.
- 81 M. S. Maru, S. Ram, J. H. Adwani and R. S. Shukla, *ChemistrySelect*, 2017, **2**, 3823–3830.
- 82 X. Nie, X. Jiang, H. Wang, W. Luo, M. J. Janik, Y. Chen, X. Guo and C. Song, *ACS Catal.*, 2018, **8**, 4873–4892.
- 83 R. K. Rai, K. Gupta, D. Tyagi, A. Mahata, S. Behrens, X. Yang, Q. Xu, B. Pathak and S. K. Singh, *Catal. Sci. Technol.*, 2016, **6**, 5567–5579.
- 84 C. J. Baddeley, *Chem. Phys. Solid Surf.*, 2002, **10**, 495–526.
- 85 E. Nowicka and M. Sankar, *J. Zhejiang Univ., Sci., A*, 2018, **19**, 5–20.
- 86 P. W. Tasker, *J. Phys. Chem. C*, 1979, **12**, 4977–4984.
- 87 T. Wang, X. Tian, Y. Yang, Y.-W. Li, J. Wang, M. Beller and H. Jiao, *Surf. Sci.*, 2016, **651**, 195–202.
- 88 D. J. Moon and J. W. Ryu, *Catal. Lett.*, 2004, **92**, 17–24.
- 89 D. J. Morgan, *Surf. Interface Anal.*, 2015, **47**, 1072–1079.
- 90 J. Zhang, K. Gao, S. Wang, W. Li and Y. Han, *RSC Adv.*, 2017, **7**, 6447–6456.
- 91 H. Wiener, J. Blum, H. Feilchenfeld, Y. Sasson and N. Zalmanov, *J. Catal.*, 1988, **110**, 184–190.
- 92 C. J. Stalder, S. Chao, D. P. Summers and M. S. Wrighton, *J. Am. Chem. Soc.*, 1983, **105**, 6318–6320.
- 93 Á. Kathó, Z. Opre, G. Laurenczy and F. Joó, *J. Mol. Catal. A: Chem.*, 2003, **204–205**, 143–148.
- 94 M. M. Taqui Khan, S. B. Halligudi and S. Shukla, *J. Mol. Catal.*, 1989, **57**, 47–60.
- 95 F. Gassner and W. Leitner, *J. Chem. Soc., Chem. Commun.*, 1993, 1465.

